Inorg. Chem. **2003**, *42*, 3565–3575

A Resonance Raman, Surface-Enhanced Resonance Raman, IR, and ab Initio Vibrational Spectroscopic Study of Nickel(II) Tetraazaannulene Complexes

Stephen Bell,[†] Joe A. Crayston,*[,‡] Trevor J. Dines,*[,†] Saira B. Ellahi,[†] and Caroline I. Smith[†]

Division of Physical & Inorganic Chemistry, Carnelley Building, University of Dundee, Dundee, Scotland, DD1 4HN, and School of Chemistry, University of St. Andrews, Fife, Scotland, KY16 9ST

Received November 27, 2002

The IR and resonance Raman spectra of the nickel(II) complexes of dibenzo[*b*,*i*][1,4,8,11]tetraaza[14]annulene (TAA) and 5,7,12,14-tetramethyldibenzo[*b*,*i*][1,4,8,11]tetraaza[14]annulene (TMTAA) have been measured and compared with ab initio calculations of the vibrational wavenumbers at the B3-LYP level using the LanL2DZ basis set. An excellent fit is found between the experimental and calculated data, enabling precise vibrational assignments to be made. Surface-enhanced resonance Raman spectra were obtained following adsorption on Ag electrodes, with potentials in the range –0.1 to –1.1 V vs Ag/AgCl. There is evidence for contributions from both the electromagnetic and charge transfer (CT) surface enhancement mechanisms. The data indicate that variations in band intensities with electrode potential can be interpreted in terms of the CT mechanism.

Introduction

In the last two decades synthetic unsaturated N_4-macrocycle complexes have been widely used as models to understand the behavior of naturally occurring macrocycles such as porphyrins. Of the many spectroscopic techniques deployed to study such systems resonance Raman (RR) spectroscopy has emerged as one of the most powerful.[1] The RR technique is ideal for studying the interaction of macrocyclic complexes with metal surfaces, where the high sensitivity enables detection at surface concentrations in the region of one monolayer. Interaction with certain metal surfaces, notably copper, silver, and gold, leads to surface-enhanced Raman scattering (SERS) resulting in a further increase of Raman signal by up to 5−6 orders of magnitude.[2−4] The combined effect of resonance and surface enhancement (surface-enhanced resonance Raman scattering, SERRS) can be as great as 10−12 orders of magnitude.

Several metalloporphyrin and synthetic N_4-macrocycle complexes have been postulated as electrocatalysts, on account of their readiness to undergo electron transfer at either the metal center or the macrocycle ring π electron system. The redox properties of dibenzo[*b*,*i*][1,4,8,11]tetraaza-[14]annulene (TAA) complexes[5] are similar to those of porphyrins although TAA complexes undergo ligand oxidation more readily, rendering these complexes more useful for electrochemical reductions than oxidations. For example, [Co^{II}TAA] is even more active for O_2 reduction than the porphyrin or phthalocyanine complexes, catalyzing the reduction of O_2 to H_2O_2 at potentials 400 mV more positive than for [CoPc].[6] TAA complexes have attracted a lot of interest in the electrochemistry area.[7] In this paper we report the results from vibrational analyses of nickel(II) complexes of TAA and its tetramethyl derivative, 5,7,12,14-tetramethyldibenzo[*b*,*i*][1,4,8,11]tetraaza[14]annulene (TMTAA), whose structures are shown in Figure 1. This study is a sequel to a previous reported RR and SERRS investigation of the

* Authors for correspondence. E-mail: jac@st-andrews.ac.uk (J.A.C.); t.j.dines@dundee.ac.uk (T.J.D.).
[†] University of Dundee.
[‡] University of St. Andrews.

(1) Clark, R. J. H.; Dines, T. J. *Angew. Chem., Int. Ed. Engl.* **1986**, *25*, 131.
(2) Creighton, J. A. In *Spectroscopy of Surfaces*; Clark, R. J. H., Hester, R. E., Eds.; Wiley: Chichester; 1988.
(3) Otto, A. In *Light Scattering in Solids IV, Topics in Applied Physics*; Cardona, M., Guntherodt, G., Eds.; Springer-Verlag: Berlin, 1984; Vol. 54, p 289.
(4) Moskovits, M *Rev. Mod. Phys.* **1985**, *57*, 783.
(5) Lukes, P. J.; McGregor, A. C.; Crayston, J. A. *Inorg. Chem.* **1992**, *31*, 4697 and references therein.
(6) Van der Putten, A.; Elzing, A.; Visscher, W.; Barendrecht, E. *J. Electroanal. Chem.* **1987**, *221*, 95.
(7) Gouerec, P.; Savy, M.; Riga, P. *Electrochim. Acta* **1998**, *43*, 743.

10.1021/ic026216e CCC: $25.00
Published on Web 05/03/2003

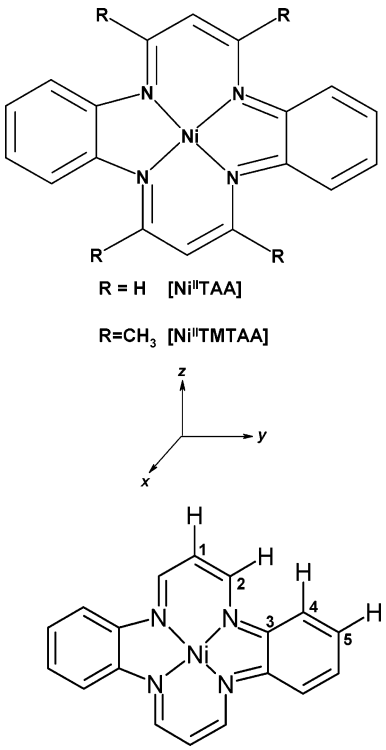

Figure 1. The structures of [Ni^{II}TAA] and [Ni^{II}TMTAA] and the atom-numbering scheme.

free ligands.[8] The nickel(II) complexes have not been subjected to intensive investigation. The literature is limited to a RR study of some metal complexes of H_2TMTAA reported in 1976,[9,10] and more recently a spectroelectrochemical study of [Co^{II}TAA].[11] In those studies, many of the vibrational assignments are open to question, and a central objective of our work has been to achieve detailed assignments making use of ab initio calculations to model IR and RR spectra.

Two recent ab initio studies of the electronic structure of [Ni^{II}TAA] have provided the basis for the electronic band assignments in this complex.[12,13] As in metalloporphyrin and phthalocyanine complexes the electronic spectrum is dominated by in-plane-polarized $\pi-\pi^*$ transitions, but these are markedly shifted from their positions in the spectrum of the free TAA ligand. In the visible region there are a doublet of weak bands at 469 and 504 nm and a strong sharp band at 426 nm with a shoulder at 404 nm. The similarity to the spectra of metalloporphyrins has led to the adoption of the same labels, i.e., Q (α = 504 nm, β = 469 nm) and Soret (426 nm). However, the analogy is an unfortunate one since these bands have different assignments from those in the higher symmetry metalloporphyrins (D_{4h}), where both Q and Soret bands are attributed to $^1E_u \leftarrow {}^1A_{1g}$ transitions which interact via configuration interaction. Furthermore, the β band in metalloporphyrins is a composite of 0−1 vibronic sidebands to the α (0−0) band. In [Ni^{II}TAA] the "α" and "β" bands are attributed to two different electronic transitions of the type $^1B_{3u} \leftarrow {}^1A_g$, and the "Soret" transition is of the type $^1B_{2u} \leftarrow {}^1A_g$. It is therefore to be expected that the pattern of RR band activity in [Ni^{II}TAA] will not bear any similarity to the spectra of metalloporphyrins, and this point is addressed in this paper.

Experimental Section

Both complexes were prepared using template synthesis methods.[14,15] For solid-state IR, UV−visible, and RR measurements KCl disks were prepared by grinding a mixture of the complex with KCl (ca. 1:100 mass) and subjecting this to a pressure of 24 MN m^{-2}. For Raman measurements these disks were mounted on a spinning sample holder and rotated at ca. 2000 rpm to minimize thermal decomposition at the laser focus. Solution Raman measurements were obtained from dichloromethane solutions (ca. 10^{-3} mol dm^{-3}) contained in glass capillary tubes. SERRS measurements were made using an electrochemical cell constructed in our own workshops, which was described in a previous publication.[8] Before electrochemical roughening (ca. 10 oxidation−reduction cycles (ORCs) through −0.6 to +0.3 V) the silver electrode was polished with a series of diamond pastes of increasingly smaller grain size (coarse, medium, and fine). Solutions of [Ni^{II}TAA] or [Ni^{II}TMTAA] in tetrahydrofuran (ca. 6 μL of a 10 mg cm^{-3} solution) were droplet-evaporated onto the roughened silver electrode surface.

Raman spectra were recorded on a Spex 1403 spectrometer controlled by a DM1B data station, using argon ion laser excitation in the range 457.9−528.7 nm (Coherent Radiation Innova 90-6) and dye laser excitation at 613.6 nm (Coherent Radiation 590 dye laser, employing DCM as the lasing medium). The laser power at the sample was maintained below 50 mW to minimize sample decomposition. Detection was by photon counting using a Hamamatsu R928 photomultiplier. All spectra were recorded with a spectral slit width in the range 2−3 cm^{-1} and corrected for the spectral sensitivity of the spectrometer. The spectrometer calibration was checked by reference to the neon emission spectrum. Depolarization ratios were measured with 90° scattering geometry ($\rho_\perp(\pi/2)$) by analyzing the scattered radiation using a Polaroid linear polarizer inserted prior to the spectrometer collection optics. The correct orientation of the polarizer was established by verifying that the dichloromethane 740 cm^{-1} band had $\rho_\perp(\pi/2) = 0.75$.

IR spectra were recorded on a Perkin-Elmer 1750 FTIR spectrometer, and UV−visible absorption spectra were measured on a Perkin-Elmer Lambda 16 spectrophotometer.

Results and Discussion

Ab Initio Calculations. Crystallographic studies have established a planar geometry for [Ni^{II}TAA];[16] the molecular geometry is therefore D_{2h}. Ab initio calculations were performed using the *Gaussian 98* program,[17] initially at the Hartree−Fock (HF-SCF) level with the 3-21G and LanL2DZ basis sets. The latter includes the Dunning−Huzinaga double-ζ basis functions (DZ)[18] for C, H, and N and the Los

(8) Bell, S.; Crayston, J. A.; Dines, T. J.; Ellahi, S. B. *J. Phys. Chem.* **1996**, *100*, 5252.
(9) Woodruff, W. H.; Pastor, R. W.; Dabrowiak, J. C. *J. Am. Chem. Soc.* **1976**, *98*, 7999.
(10) Nafie, L. A.; Pastor, R. W.; Dabrowiak, J. C.; Woodruff, W. H. *J. Am. Chem. Soc.* **1976**, *98*, 8007.
(11) Holze, R. *Z. Phys. Chem.* **1993**, *185*, 1.
(12) Rosa, A.; Ricciardi, G.; Lelj, F.; Chizhov, Y. *Chem. Phys.* **1992**, *161*, 127.
(13) Casarin, M.; Ciliberto, E.; Di Bella, S.; Gulino, A.; Fragala I.; Marks, T. J. *Inorg. Chem.* **1992**, *31*, 2835.
(14) Chipperfield, J. R.; Woodward, S. *J. Chem. Educ.* **1994**, *71*, 75.
(15) Cutler, A. R.; Dolphin, D. *J. Coord. Chem.* **1976**, *6*, 59.
(16) Weiss, M. C.; Gordon, G.; Goedken, V. I. *Inorg. Chem.* **1977**, *16*, 305.

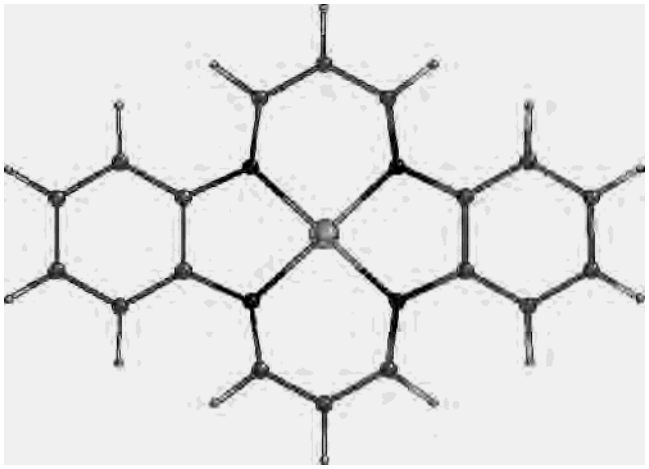

Figure 2. Optimized molecular geometry for [Ni^{II}TAA].

Alamos effective core potential for the Ni core electrons with DZ functions for Ni valence orbitals.[19] Subsequently, the molecular geometry was optimized using the hybrid SCF-density functional method commonly known as B3-LYP, which incorporates Becke's three-parameter hybrid functional[20] and the Lee, Yang, and Parr correlation functional.[21] The optimized geometry for [Ni^{II}TAA] is shown in Figure 2, and the calculated bond lengths and interbond angles are compared with the experimental values in Table 1, using the atom-numbering scheme given in Figure 1. It is evident that, although all four sets of calculated data give a reasonable fit to the experimental data, the B3-LYP/3-21G calculation gives the best fit to the bond distances, whereas the B3-LYP/LanL2DZ calculation more accurately reproduces the interbond angles.

The vibrational spectrum of [Ni^{II}TAA] was calculated at the optimized geometry using the HF-SCF and B3-LYP methods with the 3-231G and LanL2DZ basis sets. There are 105 vibrational modes, which are classified as follows:

$$\Gamma_{3N-6} = 18A_g(R,ip) + 7B_{1g}(R,op) + 9B_{2g}(R,op) + 17B_{3g}(R,ip) + 8A_u(inactive,op) + 18B_{1u}(IR,ip) + 18B_{2g}(IR,ip) + 10B_{3u}(IR,op)$$

where ip and op represent in-plane and out-of-plane, respectively, R signifies Raman activity, and IR infrared activity. Vibrations calculated at the HF-SCF level are higher than the experimental data (vide infra) by ca. 10−15%, and it is clear that B3-LYP calculations give significantly better results. The neglect of electron correlation in the HF-SCF method is a major cause of error which is to a large extent eliminated in the hybrid SCF-DFT calculations, although for proper comparison with experimental spectra scaling of the calculated force field is necessary even with the B3-LYP method. In our B3-LYP calculations, force constants involving motion of hydrogen atoms were scaled by 0.90 and all other force constants by 0.95.

Table 1. Comparison of Calculated Bond Lengths (Å) and Interbond Angles (deg) of [Ni^{II}(TAA)] with Experimental Data from X-ray Crystal Structure Analysis

		HF−SCF		B3-LYP	
	exptl[a]	3-21G	LanL2DZ	3-21G	LanL2DZ
r(NiN)	1.870	1.896	1.929	1.830	1.900
r(NC2)	1.326	1.309	1.318	1.339	1.340
r(NC3)	1.418	1.414	1.420	1.424	1.425
r(C1C2)	1.386	1.385	1.398	1.385	1.401
r(C3C4)	1.396	1.386	1.396	1.399	1.411
r(C3C3′)	1.400	1.400	1.409	1.402	1.417
r(C4C5)	1.390	1.383	1.393	1.393	1.405
r(C5C5′)	1.382	1.381	1.392	1.397	1.409
r(C1H1)	0.968	1.070	1.070	1.081	1.084
r(C2H2)	0.965	1.075	1.075	1.084	1.089
r(C4H3)	0.976	1.070	1.070	1.081	1.085
r(C5H4)	0.963	1.072	1.072	1.083	1.087
θ(NNiN′)[b]	85.2	85.5	84.8	86.2	85.1
θ(NNiN″)[b]	94.8	94.5	95.2	93.8	94.9
θ(NiNC2)	126.0	125.2	124.3	127.6	125.5
θ(NiNC3)	113.9	112.7	112.7	114.2	113.6
θ(CNC)	120.2	122.1	122.9	118.1	120.9
θ(NC3C4)	126.6	126.1	125.8	127.5	126.4
θ(NC3C3′)	113.6	114.5	114.8	112.7	113.9
θ(NC2C1)	124.7	125.8	125.7	124.6	125.2
θ(C2′C1C2)	123.8	123.6	124.7	121.7	123.7
θ(C3C4C5)	119.6	120.8	120.7	120.1	120.1
θ(C4C3C3′)	119.9	119.3	119.4	119.8	119.8
θ(C4C5C5′)	120.5	119.9	119.9	120.1	120.1
θ(C2C1H1)	118.1	118.2	117.6	119.1	118.1
θ(C1C2H2)	117.8	115.5	115.3	117.3	116.5
θ(C3C4H3)	119.9	120.7	120.9	121.2	121.2
θ(C4C5H4)	119.7	119.7	119.7	119.7	119.7

[a] Reference 16. These are averaged values; in the solid state [Ni^{II}(TAA)] has lower symmetry. [b] N and N′ are a pair of N atoms attached to a benzene ring, and N and N″ are a pair forming an imine ring.

For computation of the potential energy distributions associated with the vibrational modes, the Cartesian force constants obtained from the *Gaussian 98* output were converted to force constants expressed in terms of internal coordinates and scaled before input to a normal coordinate analysis program derived from those of Schachtschneider.[22] Symmetry-adapted linear combinations of internal coordinates were constructed according to the symmetry elements of the D_{2h} point group. Wilson symmetry coordinates were used for the CC stretching and in-plane and out-of-plane ring deformations of the benzene rings.[23] Symmetry coordinates for the 5- and 6-membered chelate rings were constructed according to the recommendations of Pulay.[24] The unscaled and scaled vibrational wavenumbers from the B3-LYP/

(17) Frisch, M. J.; Trucks, G. W.; Schlegel, H. B.; Scuseria, G. E.; Robb, M. A.; Cheeseman, J. R.; Zakrzewski, V. G.; Montgomery, J. A., Jr.; Stratmann, R. E.; Burant, J. C.; Dapprich, S.; Millam, J. M.; Daniels, A. D.; Kudin, K. N.; Strain, M. C.; Farkas, O.; Tomasi, J.; Barone, V.; Cossi, M.; Cammi, R.; Mennucci, B.; Pomelli, C.; Adamo, C.; Clifford, S.; Ochterski, J.; Petersson, G. A.; Ayala, P. Y.; Cui, Q.; Morokuma, K.; Malick, D. K.; Rabuck, A. D.; Raghavachari, K.; Foresman, J. B.; Cioslowski, J.; Ortiz, J. V.; Stefanov, B. B.; Liu, G.; Liashenko, A.; Piskorz, P.; Komaromi, I.; Gomperts, R.; Martin, R. L.; Fox, D. J.; Keith, T.; Al-Laham, M. A.; Peng, C. Y.; Nanayakkara, A.; Gonzalez, C.; Challacombe, M.; Gill, P. M. W.; Johnson, B.; Chen, W.; Wong, M. W.; Andres, J. L.; Gonzalez, C.; Head-Gordon, M.; Replogle, E. S.; Pople, J. A.; *Gaussian 98*, revision A.5; Gaussian, Inc.: Pittsburgh, PA, 1998.
(18) Dunning, T. H., Jr;. Hay, P. J. In *Modern Theoretical Chemistry*; Schaefer, H. F., III, Ed.; Plenum: New York, 1976; Vol. 3, p 1.
(19) Hay, P. J.; Wadt, W. R. *J. Chem. Phys.* **1985**, *82*, 270, 284, 299.
(20) Becke, A. D. *J. Chem. Phys.* **1993**, *98*, 5648.
(21) Lee, C.; Yang W.; Parr, R. G. *Phys. Rev. B* **1988**, *37*, 785.
(22) Schachtschneider, J. A. *Vibrational Analysis of Polyatomic Molecules*; Parts V and VI; Technical Reports, No. 231 and 57; Shell Development Co.: Houston, TX; 1964 and 1965.
(23) Varsányi, *G. Vibrational Spectra of Benzene Derivatives*; Academic Press: New York; 1969.

Table 2. Vibrational Spectrum of [Ni^{II}TAA] Calculated at the B3-LYP/LanL2DZ Level

	$\tilde{\nu}$/cm^{-1}		potential energy distribution (%)
	unscaled	scaled	
A_g			
ν_1	3242	3076	ν(C1H) (84)
ν_2	3236	3071	ν(C4H) (43), ν(C5H) (48)
ν_3	3212	3047	ν(C4H) (48), ν(C5H) (48)
ν_4	3173	3010	ν(C2H) (89)
ν_5	1654	1603	ν(C1C2) (10), ν(C2N) (13), S_{8a} (55), δ_{ip}(C2H) (10)
ν_6	1628	1579	ν(C1C2) (12), ν(C2N) (35), S_{8a} (23), δ_{ip}(C2H) (14)
ν_7	1533	1473	S_{19b} (38), δ_{ip}(C4H) (38)
ν_8	1411	1362	ν(C2N) (11), S_{14} (64), δ_{ip}(C2H) (15)
ν_9	1390	1346	ν(C2N) (16), S_{14} (31), δ_{ip}(C2H) (38)
ν_{10}	1286	1246	ν(C3N) (42), S_{8a} (18)
ν_{11}	1215	1157	δ_{ip}(C4H) (25), δ_{ip}(C5H) (62)
ν_{12}	1102	1068	ν(C1C2) (49), S_{19b} (17)
ν_{13}	1068	1032	ν(C1C2) (11), S_1 (14), S_{19b} (34), δ_{ip}(C4H) (18)
ν_{14}	978	950	S_1 (35), 5-ring def.1 (47)
ν_{15}	748	725	ν(C3N) (20), S_1 (20), ν (NiN) (16), S_{6a} (11), 6-ring def.3 (17)
ν_{16}	632	612	ν (NiN) (22), S_{6a} (67)
ν_{17}	412	401	ν(C2N) (10), ν(NiN) (44), S_{6a} (10), 5,6-ring def.1 (17)
ν_{18}	234	227	5,6-ring def.1 (62) 6-ring def.3 (16)
B_{1g}			
ν_{19}	984	932	δ_{op}(C2H) (93)
ν_{20}	967	915	δ_{op}(C2H) (11), δ_{op}(C4H) (64), δ_{op}(C5H) (33)
ν_{21}	776	738	δ_{op}(C4H) (28), δ_{op}(C5H) (63)
ν_{22}	496	482	δ_{op}(C3N) (41), S_{16b} (23), 5-ring tor.2 (29)
ν_{23}	394	384	S_{16b} (58), 5-ring tor.2 (20), 6-ring tor.2 (30)
ν_{24}	253	246	δ_{op}(C3N) (12), S_{16b} (30), 6-ring tor.2 (63)
ν_{25}	107	105	δ_{op}(C3N) (36), 5-ring tor.2 (50), 6-ring tor.2 (13)
B_{2g}			
ν_{26}	1013	955	δ_{op}(C4H) (27), δ_{op}(C5H) (91)
ν_{27}	985	930	δ_{op}(C1H) (32), δ_{op}(C2H) (17)
ν_{28}	884	841	δ_{op}(C4H) (67), δ_{op}(C5H) (17)
ν_{29}	797	764	δ_{op}(C1H) (40), S_4 (32), 5-ring tor.1 (15)
ν_{30}	765	739	δ_{op}(C1H) (31), δ_{op}(C2H) (11), S_4 (28), 5-ring tor.1 (10), 6-ring tor.1 (12)
ν_{31}	582	569	S_4 (37), S_{16a} (49), 5-ring tor.1 (25)
ν_{32}	533	520	6-ring tor.1 (65), 6-ring tor.3 (35)
ν_{33}	316	307	S_{16a} (31), 6-ring tor.1 (12), 6-ring tor.3 (48)
ν_{34}	80	78	S_{16a} (24), 5-ring tor.1 (33), 6-ring tor.1 (14), 6-ring tor.3 (22)
B_{3g}			
ν_{35}	3226	3061	ν(C4H) (83), ν(C5H) (13)
ν_{36}	3197	3033	ν(C4H) (12), ν(C5H) (86)
ν_{37}	3174	3012	ν(C2H) (94)
ν_{38}	1639	1589	S_{8b} (62), δ_{ip}(C4H) (12)
ν_{39}	1561	1510	ν(C1C2) (62), δ_{ip}(C1H) (18)
ν_{40}	1502	1442	ν(C2N) (33), S_{19a} (11), δ_{ip}(C1H) (13), δ_{ip}(C2H) (22), δ_{ip}(C5H) (11)
ν_{41}	1486	1423	S_{19a} (25), δ_{ip}(C2H) (22), δ_{ip}(C5H) (31)
ν_{42}	1354	1299	ν(C2N) (27), δ_{ip}(C2H) (42), δ_{ip}(C5H) (11)
ν_{43}	1319	1266	δ_{ip}(C4H) (50)
ν_{44}	1272	1226	ν(C3N) (32), S_{12} (10), δ_{ip}(C1H) (34)
ν_{45}	1187	1137	S_{8b} (10), δ_{ip}(C1H) (20), δ_{ip}(C4H) (17), δ_{ip}(C5H) (21)
ν_{46}	1117	1079	S_{12} (39), S_{19a} (19), δ_{ip}(C5H) (10)
ν_{47}	895	868	ν(C3N) (17), S_{12} (44), 6-ring def.2 (18)
ν_{48}	678	659	ν(NiN) (13), S_{6b} (42), 6-ring def.2 (20)
ν_{49}	572	555	S_{19a} (11), 5-ring def.2 (58), 6-ring def.2 (10)
ν_{50}	370	359	ν(C3N) (12), ν(NiN) (20), S_{6b} (17), 6-ring def.2 (41)
ν_{51}	285	278	ν(C3N) (10), ν(NiN) (54), S_{6b} (20)
A_u			
ν_{52}	1013	955	δ_{op}(C4H) (27), δ_{op}(C5H) (90)
ν_{53}	984	932	δ_{op}(C2H) (99)
ν_{54}	884	842	δ_{op}(C4H) (67), δ_{op}(C5H) (17)
ν_{55}	771	750	S_4 (60), 5-ring tor.1 (24)
ν_{56}	576	564	S_4 (40), S_{16a} (45), 5-ring tor.1 (24)
ν_{57}	373	364	τ(C2NC3C4) (41), S_{16a} (30), 6-ring tor.2 (26)
ν_{58}	183	178	S_4 (11), S_{16a} (34), 6-ring tor.2 (83)
ν_{59}	79	77	τ (C2NC3C4) (73), 5-ring tor.1 (33)
B_{1u}			
ν_{60}	3242	3076	ν(C1H) (90)
ν_{61}	3226	3061	ν(C4H) (83), ν(C5H) (13)
ν_{62}	3197	3033	ν(C4H) (12), ν(C5H) (86)
ν_{63}	3172	3010	ν(C2H) (89)
ν_{64}	1642	1591	ν(C1C2) (13), ν(C2N) (32), S_{8b} (28), δ_{ip}(C2H) (13)
ν_{65}	1631	1578	ν(C2N) (16), S_{8b} (42), δ_{ip}(C2H) (11), δ_{ip}(C4H) (10)
ν_{66}	1487	1428	S_{19a} (37), ,$_{ip}$(C5H) (42), 5-ring def.2 (11)
ν_{67}	1404	1348	ν(C2N) (26), δ_{ip}(C2H) (52)
ν_{68}	1336	1279	δ_{ip}(C4H) (57), δ_{ip}(C5H) (11)
ν_{69}	1253	1211	ν(C1C2) (11), ν(C3N) (34), S_{8b} (13), S_{12} (10), δ_{ip}(C4H) (10), δ_{ip}(C5H) (14)
ν_{70}	1149	1105	S_{19a} (23), S_{12} (14), δ_{ip}(C4H) (12), δ_{ip}(C5H) (25)
ν_{71}	1081	1047	ν(C1C2) (43), 6-ring def.3 (18)
ν_{72}	991	960	S_{12} (43), 6-ring def.3 (43)
ν_{73}	786	761	ν(C3N) (20), S_{6b} (22), S_{12} (16), 6-ring def.1 (10), 6-ring def.3 (15)
ν_{74}	653	636	ν (NiN) (34), S_{6b} (20), 5-ring def.2 (23)
ν_{75}	522	507	S_{6b} (25), 5-ring def.2 (38), 6-ring def.1 (12)
ν_{76}	399	389	ν(NiN) (47), 6-ring def.1 (25)
ν_{77}	177	173	ν(C3N) (13), S_{6b} (17), 6-ring def.1 (38), 6-ring def.3 (13)
B_{2u}			
ν_{78}	3236	3071	ν(C4H) (48), ν(C5H) (50)
ν_{79}	3212	3048	ν(C4H) (47), ν(C5H) (49)
ν_{80}	3175	3012	ν(C2H) (95)
ν_{81}	1647	1600	S_{8a} (66)
ν_{82}	1585	1535	ν(C1C2) (60), S_{8a} (12)
ν_{83}	1538	1483	ν(C1C2) (29), ν(C3N) (11), S_{19b} (14), δ_{ip}(C2H) (12), δ_{ip}(C4H) (19)
ν_{84}	1496	1433	ν(C2N) (19), S_{19b} (19), δ_{ip}(C1H) (23), δ_{ip}(C4H) (21)
ν_{85}	1394	1346	S_{14} (77)
ν_{86}	1376	1327	ν(C2N) (19), S_{19b} (17), δ_{ip}(C1H) (58)
ν_{87}	1297	1252	ν(C3N) (40), S_1 (14), δ_{ip}(C1H) (20)
ν_{88}	1212	1154	δ_{ip}(C4H) (25), δ_{ip}(C5H) (63)
ν_{89}	1182	1137	ν(C1C2) (11), ν(C2N) (15), δ_{ip}(C1H) (42)
ν_{90}	1072	1037	S_1 (25), S_{19b} (44), δ_{ip}(C4H) (17)
ν_{91}	892	868	ν(C3N) (12), S_1 (38), ν(NiN) (13), 6-ring def.2 (25)
ν_{92}	657	636	S_{6a} (70), ν(NiN) (11)
ν_{93}	496	482	ν(NiN) (57), 5-ring def.1 (15), 6-ring def.2 (17)
ν_{94}	424	413	ν(C3N) (25), S_1 (11), S_{6a} (13), 6-ring def.2 (33)
ν_{95}	367	358	5-ring def.1 (71)
B_{3u}			
ν_{96}	989	933	δ_{op}(C1H) (29), δ_{op}(C2H) (81)
ν_{97}	969	916	δ_{op}(C4H) (68), δ_{op}(C5H) (34)
ν_{98}	793	754	δ_{op}(C1H) (70), δ_{op}(C2H) (14), 6-ring tor.1 (11)
ν_{99}	777	740	δ_{op}(C4H) (26), δ_{op}(C5H) (60)
ν_{100}	569	555	6-ring tor.1 (101), 6-ring tor.3 (10)
ν_{101}	516	502	δ_{op}(C3N) (32), S_{16b} (11), δ_{op}(NiN) (10), 5-ring tor.2 (26), 6-ring tor.3 (12)
ν_{102}	396	387	S_{16b} (72), 6-ring tor.3 (25)
ν_{103}	241	235	δ_{op}(C3N) (34), S_{16b} (25), 6-ring tor.3 (33)
ν_{104}	106	103	δ_{op}(C3N)(15), δ_{op}(NiN) (108), 5-ring tor.2 (15)
ν_{105}	2	2	5-ring tor.2 (39), 6-ring tor.1 (23), 6-ring tor.3 (41)

LanL2DZ calculation are listed in Table 2, together with the potential energy distributions, determined using the scaled force field. Only symmetry coordinates contributing ≥10% to the potential energy distribution have been included in the list. Examination of the potential energy distributions reveals that many vibrations involve both the diimine and benzene ring chromophores. Nevertheless, it is found that many of the CC and CN stretches and deformations and the

CH deformations can be clearly identified with either the diimine or benzene ring parts of the molecule. In the region below 1700 cm^{-1} there is less mixing of the symmetry coordinates and in fact many of the vibrations associated with the benzene rings are within the ranges expected for ortho-substituted benzene.[23,25]

Due to steric hindrance between the methyl groups and ortho-hydrogen atoms the H_2TMTAA ligand and its Ni^{II} complex have a nonplanar saddle-shaped structure, with C_{2v} symmetry.[26,27] Nevertheless, it was found that the IR and RR spectra of [Ni^{II}TMTAA] showed sufficient similarity to those of the TAA complex that the molecular vibrations may be interpreted in terms of full D_{2h} symmetry, in the same way that the RR spectra of substituted and nonplanar metalloporphyrin derivatives can be assigned in terms of D_{4h} symmetry.[28,29]

Electronic Spectra. The electronic absorption spectra of [Ni^{II}TAA] and [Ni^{II}TMTAA] in THF solution and in the solid state are presented in Figure 3; the band positions and assignments are listed in Table 3. Both complexes display an intense band in the near-UV and a less intense band in the visible region, both of which are considerably red-shifted relative to the analogous bands of the free ligands. In [Ni^{II}-TAA], as was also the case for the free TAA ligand,[8] both bands appear as doublets. The separations between the first pair of bands in the visible region (1680 cm^{-1}) and the second pair in the near-UV (1390 cm^{-1}) are not constant and vary markedly upon complexation. Several electric-dipole-allowed transitions are predicted, and by contrast to porphyrins, where such splitting is attributed to vibronic structure,[30] the four bands of [Ni^{II}TAA] are identified with four individual electronic transitions,[12] all of which are polarized in the molecular plane. In Table 3 we have listed the assignments given by Rosa et al.[12] but, since these have been derived using a nonstandard set of Cartesian axes, we have also listed these in terms of the symmetry species relating to the standard Cartesian coordinate system for the D_{2h} point group. Three of the four observed transitions are polarized in the plane of the molecule, along the *y*-axis. However, one transition is *z*-polarized, i.e., perpendicular to the molecular plane, and this has important consequences for the RR scattering mechanism. Electronic absorption spectra of the Ni(II) and Cu(II) complexes of TAA and TMTAA have also been reported by Snopok and Lampeka,[31] for solutions in ethanol at room temperature and 77 K. Their assignments differ from those of Rosa et al. but have been assumed to be identical for both the Cu(II) and Ni(II) complexes and are not supported by ab initio calculations.

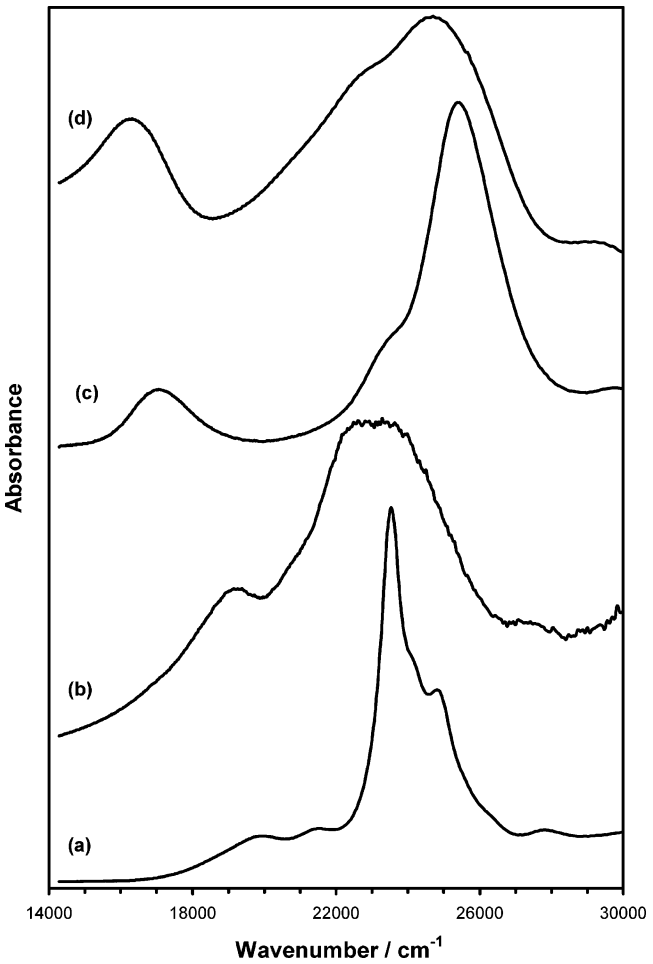

Figure 3. Electronic absorption spectra of [Ni^{II}TAA] in (a) THF solution and (b) the solid state and of [Ni^{II}TMTAA] in (c) THF solution and (d) the solid state.

Table 3. Electronic Absorption Band Positions and Assignments

wavenumber/cm^{-1}				assignment		
[Ni^{II}TAA]		[Ni^{II}TMTAA]				
soln	solid	soln	solid	Rosa et al.[7]	std notation	
19881	18939	17036	16502	$4b_{3g} \rightarrow 3a_u$	$b_{2g} \rightarrow a_u$	$^1B_{2u} \leftarrow {}^1A_g$ (y)
21505	20619			$5b_{1u} \rightarrow 5b_{2g}$	$b_{3u} \rightarrow b_{2g}$	$^1B_{2u} \leftarrow {}^1A_g$ (y)
23529	22472	23148	22472	$4b_{2g} \rightarrow 3a_u$	$b_{2g} \rightarrow a_u$	$^1B_{1u} \leftarrow {}^1A_g$ (z)
(24213)						
24814	23866	25381	25000	$3b_{3g} \rightarrow 3a_u$	$b_{2g} \rightarrow a_u$	$^1B_{2u} \leftarrow {}^1A_g$ (y)

In common with the spectra of the free ligands,[8] the solid-state spectra for both [Ni^{II}TAA] and [Ni^{II}TMTAA] are red-shifted with respect to the solution spectra. The analysis of Rosa et al. concluded that the optical spectrum of [Ni^{II}TAA] was due to transitions leading to a charge rearrangement within the macrocycle as in the case of porphyrins. However, most of the transitions originate from orbitals involved in π-metal−macrocycle interactions (with large metal contributions, 78% for the higher energy band and 61% for the lower). This is in contrast to the porphyrins where the visible and near-UV bands are due to transitions originating from almost pure ring orbitals. These differences are attributed to the shorter metal−nitrogen bond distance, resulting in an increased delocalization of $d_{x^2-y^2}$ orbitals in [Ni^{II}TAA]

(24) Pulay, P.; Fogarasi, G.; Pang, F.; Boggs, J. E. *J. Am. Chem. Soc.* **1979**, *101*, 2550.
(25) Dollish, F. R.; Fateley, W. G.; Bentley, F. F. *Characteristic Raman Frequencies of Organic Compounds*; Wiley-Interscience: New York, 1974.
(26) Goedken, V. L.; Molin-Case, J.; Whang, Y.-A. *J. Chem. Soc., Chem. Commun.* **1973**, 337.
(27) Goedken, V. L.; Park, Y.-A. *J. Chem. Soc., Chem. Commun.* **1975**, 214.
(28) Felton, R. H.; Yu, N.-T. In *The Porphyrins*; Dolphin, D., Ed.; Academic Press: New York, 1978; Vol. 3, p 347.
(29) Spiro, T. G. Czernuszewicz, R. S. *Coord. Chem. Rev.* **1990**, *100*, 541.
(30) Gouterman, M. *J. Mol. Spectrosc.* **1961**, *6*, 138.
(31) Snopok, B. A.; Lampeka, Y. D. *Opt. Spectrosc.* **1993**, *75*, 189.

Table 4. IR Band Wavenumber Positions (cm^{-1}) for [Ni^{II}TAA] and [Ni^{II}TMTAA], Calculated Band Wavenumbers, and Assignments

[Ni^{II}TAA]		[Ni^{II}TMTAA]		calcd	assignments	
		3055	vw			
		2964	w			
2927	vw	2922	w			
		2860	vw			
1654	vw, br	1654	w, br			
		1581	w	1578	$\nu_{65}(b_{1u})$	S_{8b}
		1543	s	1535	$\nu_{82}(b_{2u})$	ν(C1C2)
		1525	sh			
1461	vs	1465	vs	1483	$\nu_{83}(b_{2u})$	ν(C1C2)
		1434	m	1434	$\nu_{84}(b_{2u})$	δ_{ip}(C1H), δ_{ip}(C4H)
		1394	vs	1428	$\nu_{66}(b_{1u})$	S_{19a}, δ_{ip}(C5H)
1356	m	1364	m, sh	1348	$\nu_{67}(b_{1u})$	δ_{ip}(C2H)
1336	vs	1345	w, sh	1347	$\nu_{85}(b_{2u})$	S_{14}
1261	m	1276	m	1252	$\nu_{87}(b_{2u})$	ν(C3N)
1192	m	1207	s	1211	$\nu_{69}(b_{2u})$	ν(C3N)
		1163	vw	1154	$\nu_{88}(b_{2u})$	δ_{ip}(C5H)
1115	s	1116	m	1137	$\nu_{89}(b_{1u})$	δ_{ip}(C1H)
1044	vw	1051	vw	1037	$\nu_{90}(b_{1u})$	S_{19b}
		1034	s	1047	$\nu_{71}(b_{1u})$	ν(C1C2)
		949	vw	933	$\nu_{96}(b_{3u})$	δ_{op}(C2H)
		922	w	916	$\nu_{97}(b_{3u})$	δ_{op}(C4H)
		859	vw	868	$\nu_{91}(b_{2u})$	S_1
		766	w	754	$\nu_{98}(b_{3u})$	δ_{op}(C1H)
745	m	742	s	740	$\nu_{99}(b_{3u})$	δ_{op}(C5H)
669	m	670	w	636	$\nu_{92}(b_{2u})$	S_{6a}
637	w			636	$\nu_{74}(b_{1u})$	ν(NiN)
620	w	621	w	621	$\nu_{100}(b_{3u})$	6-ring tor.1

Table 5. Resonance Raman Band Depolarization Measurements for [Ni^{II}TAA] and [Ni^{II}TMTAA] in CH_2Cl_2 Solution

[Ni^{II}TAA]				[Ni^{II}TMTAA]		
	$\rho_\perp(\pi/2)$[a]				$\rho_\perp(\pi/2)$[a]	
$\tilde{\nu}/cm^{-1}$	514.5 nm	488.0 nm	457.9 nm	$\tilde{\nu}/cm^{-1}$	514.5 nm	457.9 nm
238	0.43	p	p	198	p	
422	p	p		252		dp
500	p	p	p	328	p	0.67
548	0.5	p		396	0.40	0.63
620	p	0.7	p	410	p	
966		p		500	p	0.30
1044	p	p	p	567	0.44	0.41
1078	0.5	0.63	p	644	p	0.33
1158	0.6	p	p	855	0.42	0.65
1254		p	0.64	965	p	p
1322	p	p	p	1015	p	p
1360	0.49	0.51	0.39	1032	dp	dp
1490	dp	dp	0.41	1058		p
1582	0.69	0.69	0.36	1142	dp	dp
1602	p	p		1250	0.53	0.36
				1288	p	0.36
				1318		p
				1376		p
				1408	p	
				1482		0.31
				1530		0.27
				1550		0.33

[a] Accurate values were not obtainable for weaker bands, and they are designated p (polarized) or dp (depolarized). Blank entries in any column signify that the band was not observed with that excitation wavelength.

compared to Ni porphyrins, as well as the fact that in [Ni^{II}TAA] there are fewer ligand π orbitals available compared to the porphyrins. It is the π-metal−macrocycle interactions which are therefore responsible for the bathochromic shift of the absorption bands of the Ni(II) complexes with respect to the free ligands.

IR Spectra. The band wavenumber positions and assignments for the IR spectra of [Ni^{II}TAA] and [Ni^{II}TMTAA] are listed in Table 4. The band assignments were obtained by comparison with the ab initio calculated band wavenumbers and potential energy distributions. There is an excellent match between the calculated and experimental data and reasonably close correspondence between the IR spectra of the two complexes, with most bands within 5−10 cm^{-1}. It is of particular significance that all the observed bands are attributable to in-plane vibrations (b_{1u} and b_{2u}). Clearly the out-of-plane modes (b_{3u}) give rise to only very weak dipole moment alterations. There is a band in the spectrum of [Ni^{II}TMTAA] at 922 cm^{-1} which has no counterpart in [Ni^{II}TAA] and could not be assigned on the basis of the ab initio calculations. We therefore believe this is attributable to a vibration associated with the methyl groups, the most likely assignment being ν(C−CH_3).

RR Spectra. RR spectra of both complexes were obtained from solutions in CH_2Cl_2 and in the solid state as KCl disks; the solid-state spectra are shown in Figures 4 and 5. For [Ni^{II}TAA] the relative intensities of several lower wavenumber bands are greater with shorter wavelength excitation (457.9 nm) and the high-wavenumber bands are stronger with longer excitation wavelengths. By contrast, the exact opposite trend is observed for [Ni^{II}TMTAA]. Solution spectra were of very poor quality, being dominated by solvent bands, and they are not reproduced here. It proved impossible to obtain spectra at higher concentrations due to strong self-absorption of the RR scattering. It is particularly significant that only very weak spectra were obtained even with solution concentrations as high as 10^{-3} mol dm^{-3}. This contrasts with the behavior exhibited by metalloporphyrins, which display intense RR spectra with excitation within either the Q or Soret bands at concentrations as low as 10^{-6} mol dm^{-3}. The feeble RR signal displayed by the TAA complexes is an indication that either (a) there is interference between the contributions to the transition polarizability from several resonant electronic transitions or (b) the resonant excited state(s) have a short lifetime, resulting in a large homogeneous bandwidth.[1]

Notwithstanding the weak solution spectra, it proved possible to obtain depolarization measurements for both complexes (Table 5), which have assisted in Raman band assignments. Most of the bands observed in the solution spectra have $\rho_\perp(\pi/2)$ significantly below 0.75 and can therefore be attributed to totally symmetric modes. For excitation resonant with a nondegenerate excited state it is predicted that $\rho_\perp(\pi/2) = {}^1/_3$ for totally symmetric modes.[1] Any deviation from this limiting value indicates a contribution to the A-term RR scattering mechanism from two or more electronic transitions, with different polarization directions. The data show that the $\rho_\perp(\pi/2)$ values vary with excitation wavelength, i.e., exhibiting polarization dispersion. We therefore propose that for excitation in the range 457.9−514.5 nm the contributing transitions are the three lowest energy electric-dipole-allowed transitions $^1B_{2u} \leftarrow {}^1A_g$ (y-polarized, 19881 and 21505 cm^{-1} in [Ni^{II}TAA]) and $^1B_{1u} \leftarrow {}^1A_g$ (z-polarized, 23529 cm^{-1}). That there are contributions from nearby excited states of different symmetry indicates that vibronic coupling may occur between these states,

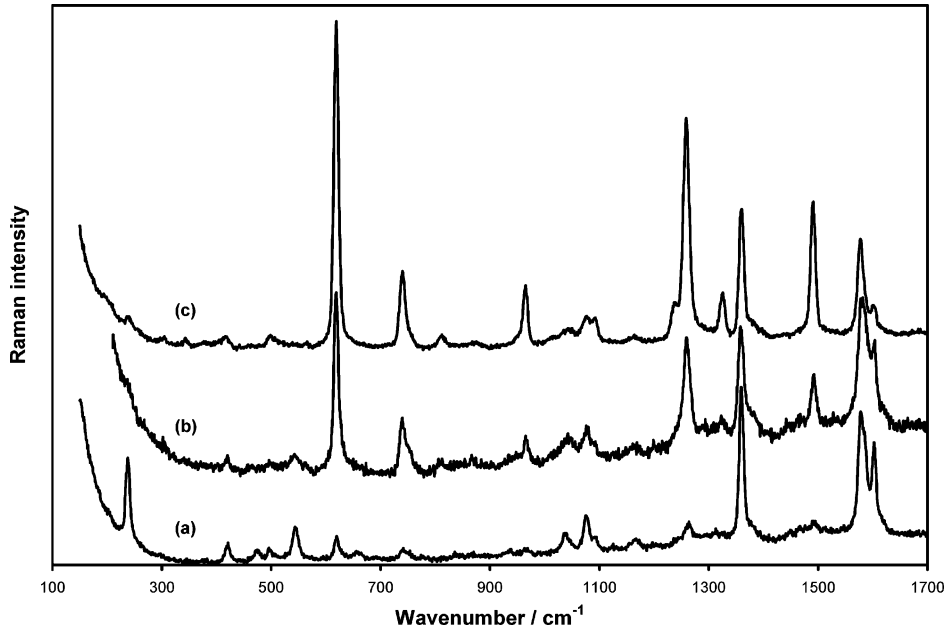

Figure 4. RR spectra of [Ni^{II}TAA] recorded with (a) 514.5, (b) 488.0, and (c) 457.9 nm excitation.

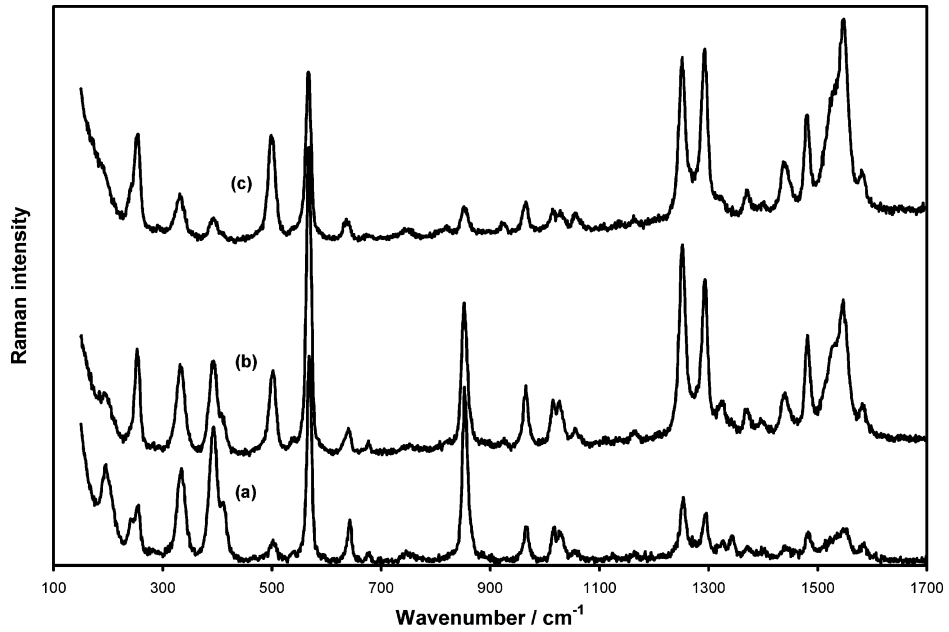

Figure 5. RR spectra of [Ni^{II}TMTAA] recorded with (a) 514.5, (b) 488.0, and (c) 457.9 nm excitation.

resulting in B-term RR scattering for nontotally symmetric modes of appropriate symmetry.[1] Vibronic coupling of $^1B_{1u}$ and $^1B_{2u}$ states is effected by in-plane vibrations of b_{3g} symmetry. It is therefore expected that the non-totally-symmetric vibrations observed in the RR spectra are mostly of b_{3g} symmetry, although the depolarization measurements do not permit distinction between the three classes of non-totally-symmetric modes. Furthermore, comparison of the observed and calculated spectra indicates that some bands must be assigned to the out-of-plane vibrations (b_{1g} and b_{2g}). In cases where there are contributions to A-term scattering from excited states of different symmetry (contributing to α_{yy} and α_{zz} in the present case) even totally symmetric modes may exhibit ρ values close to 0.75. This is especially probable if the preresonant contribution from the $^1B_{1u} \leftarrow {}^1A_g$ transition gives rise to a α_{zz} value which is close to $-\alpha_{yy}$, the latter being dominated by the resonant $^1B_{2u} \leftarrow {}^1A_g$ transition. Our assignments of the RR spectra are therefore based partly on the polarization data but also on the ab initio predictions.

Detailed assignments of the solid-state RR spectra are given in Tables 6 and 7. For [Ni^{II}TAA] 14 of the 18 a_g vibrations are observed; the absent ones are the four totally symmetric C−H stretching modes. The three excitation wavelengths (514.5, 488.0, and 457.9 nm) span the first two absorption bands, designated I and II, which are both assigned to $^1B_{2u} \leftarrow {}^1A_g$ transitions. The 514.5 nm excitation is close to the maximum of band I, and the strongest RR bands are those in the high-wavenumber region. The strongest and third strongest bands (1359 and 1602 cm^{-1}) are associated with benzene ring stretching, the second and

Table 6. RR and SERRS Band Wavenumber Positions and Relative Intensities for [Ni^{II}TAA] and Calculated Band Wavenumbers and Assignments

	RR intensity[a]			SERRS	calcd	assignments	
$\tilde{\nu}$/cm^{-1}	514.5	488.0	457.9	$\tilde{\nu}$/cm^{-1}	$\tilde{\nu}$/cm^{-1}		
1602	58	79	22	1602	1603	$\nu_5(a_g)$	S_{8a}
1578	78	116	73	1579	1579	$\nu_6(a_g)$	ν(C2N)
1528		4		1532			
1491	7	43	102	1490	1510	$\nu_{39}(b_{3g})$	ν(C1C2)
1465	3	3		1466	1473	$\nu_7(a_g)$	S_{19b}, δ_{ip}(C4H)
1449	2	3		1457	1442	$\nu_{40}(b_{3g})$	ν(C2N)
1376		4(sh)	9	1368			
1359	100	100	100	1359	1362	$\nu_8(a_g)$	S_{14}
1325		12	31		1346	$\nu_9(a_g)$	S_{14}, δ_{ip}(C2H)
1259	9	93	169	1263	1246	$\nu_{10}(a_g)$	ν(C3N)
1237			18	1241	1226	$\nu_{44}(b_{3g})$	ν(C3N)
1167	6	6	4	1164	1157	$\nu_{11}(a_g)$	δ_{ip}(C5H)
1125	2			1123	1137	$\nu_{45}(b_{3g})$	δ_{ip}(C5H)
1092	8	4	16	1092	1079	$\nu_{46}(b_{3g})$	S_{12}
1075	24	25	16	1075	1068	$\nu_{12}(a_g)$	ν(C1C2)
1040	13	21	4	1036	1032	$\nu_{13}(a_g)$	S_{19b}
				992	987	$\nu_{26}(b_{2g})$	δ_{op}(C5H)
963	3	25	47	963	950	$\nu_{14}(a_g)$	S_1, 5-ring def.1
939	3			935	943	$\nu_{20}(b_{1g})$	δ_{op}(C4H)
870		9	2				
836	2			836	868	$\nu_{47}(b_{3g})$	S_{12}
813		6	7				
742	7	55	60	744	725	$\nu_{15}(a_g)$	ν(C3N), S_1
				689			
655	5			659	659	$\nu_{48}(b_{3g})$	S_{6b}
620	16	179	256	619	612	$\nu_{16}(a_g)$	S_{6a}
				563	569	$\nu_{31}(b_{2g})$	S_{16a}
544	24	15		542	555	$\nu_{49}(b_{3g})$	5-ring def.2
496	7	4	7	496	520	$\nu_{32}(b_{2g})$	6-ring tor.1
474	7			473	483	$\nu_{22}(b_{1g})$	δ_{op}(C3N)
421	15	12	7	418	401	$\nu_{17}(a_g)$	ν(NiN)
381			4	379	384	$\nu_{23}(b_{1g})$	S_{16b}
343			4				
305			4	293	307	$\nu_{33}(b_{2g})$	6-ring tor.3
238	61		7	238	227	$\nu_{18}(a_g)$	5,6-ring def.1

[a] Relative band intensities are normalized to a value of 100 for the 1359 cm^{-1} band in each spectrum.

fourth strongest bands (1075 and 1578 cm^{-1}) with stretching of the imine rings, principally of the C1−C2 and C2−N bonds. Thus, the major geometric changes within the first $^1B_{2u}$ excited state are associated with these parts of the molecule. Excitation at 488.0 nm leads to a decrease in signal-to-noise ratio, consistent with decreasing absorption in this region, although several bands are increased in intensity, especially those at 1491, 1259, 963, 742, and 620 cm^{-1}, reflecting the onset of resonance with the second $^1B_{2u}$ state (band II). The 1491 cm^{-1} band is of b_{3g} symmetry; its appearance is due to participation in vibronic coupling to the higher energy $^1B_{1u}$ state. Excitation in resonance with band II (457.9 nm) affords large increases in the intensities of the 1491, 1325, 1259, 1237, 963, and 620 cm^{-1} bands. With the exception of the 1491 and 1237 cm^{-1} bands (b_{3g}), these are all totally symmetric vibrations. In particular, the 620 cm^{-1} band intensity increases 16-fold (relative to the 1359 cm^{-1} band) on going from 514.5 to 457.9 nm excitation. This vibration is attributed to the **6a** benzene ring deformation, with some contribution from Ni−N stretching. This indicates that there is significant distortion of the benzene rings in the second $^1B_{2u}$ state, accompanied by alteration of the Ni−N bond distances.

Table 7. RR and SERRS Band Wavenumber Positions (cm^{-1}) and Relative Intensities for [Ni^{II}TMTAA] and Calculated Band Wavenumbers and Assignments

	RR intensity[a]			SERRS	calcd	assignments	
$\tilde{\nu}$/cm^{-1}	514.5	488.0	457.9	$\tilde{\nu}$/cm^{-1}	$\tilde{\nu}$/cm^{-1}		
1582	5	8	15	1578	1603	$\nu_5(a_g)$	S_{8a}
1547	11	41	113	1539	1579	$\nu_6(a_g)$	ν(C2N)
1529	sh	sh	sh	1523	1510	$\nu_{39}(b_{3g})$	ν(C1C2)
1481	9	27	49	1479	1473	$\nu_7(a_g)$	S_{19b}, δ_{ip}(C4H)
1440	4	11	26	1439	1442	$\nu_{40}(b_{3g})$	ν(C2N)
1397	1	2	2				
1370	3	7	13	1371	1362	$\nu_8(a_g)$	S_{14}
1343	7				1346	$\nu_9(a_g)$	δ_{ip}(C2H)
1325	3	6	5		1327	$\nu_{86}(b_{2u})$	δ_{ip}(C1H)
1293	18	47	99	1293	1299	$\nu_{42}(b_{3g})$	δ_{ip}(C2H), ν(C2N)
				1267	1266	$\nu_{43}(b_{3g})$	δ_{ip}(C4H)
1253	25	61	95	1250	1246	$\nu_{10}(a_g)$	ν(C3N)
1165	2	3	4	1161	1157	$\nu_{11}(a_g)$	δ_{ip}(C5H)
1125	1				1137	$\nu_{45}(b_{3g})$	δ_{ip}(C5H)
1056	4	4	9	1047	1068	$\nu_{12}(a_g)$	ν(C1C2)
1027	12	13	10	1027	1037	$\nu_{90}(b_{2u})$	S_{19b}
1015	15	14	11		1032	$\nu_{13}(a_g)$	S_{19b}
965	15	20	17	966	950	$\nu_{14}(a_g)$	S_1, 5-ring def.1
925	1	2	6		930	$\nu_{27}(b_{2g})$	δ_{op}(C1H)
853	82	48	15	853	868	$\nu_{47}(b_{3g})$	S_{12}
820			3		841	$\nu_{28}(b_{2g})$	δ_{op}(C4H)
748	4	2	5		740	$\nu_{99}(b_{3u})$	δ_{op}(C5H)
677	3	3	2		725	$\nu_{15}(a_g)$	ν(C3N), S_1
640	20	8	12	635	659	$\nu_{48}(b_{3g})$	S_{6b}
568	100	100	100	566	612	$\nu_{16}(a_g)$	S_{6a}
				557	555	$\nu_{49}(b_{3g})$	5-ring def.2
539	3	3	sh	538			
502	9	27	60	494	520	$\nu_{32}(b_{2g})$	6-ring tor.1
409	sh	sh	sh	423	413	$\nu_{94}(b_{2u})$	6-ring def.2
				404			
393	67	32	13	390	401	$\nu_{17}(a_g)$	ν(NiN)
				343	359	$\nu_{50}(b_{3g})$	6-ring def.2
333	43	30	25	332	307	$\nu_{33}(b_{2g})$	6-ring tor. 3
285	1		2	278	278	$\nu_{51}(b_{3g})$	ν(NiN)
253	23	35	53		246	$\nu_{24}(b_{1g})$	6-ring tor.2
238	sh			239	235	$\nu_{103}(b_{3u})$	δ_{op}(C3N), 6-ring tor.3
196	28	11		195	227	$\nu_{18}(a_g)$	5,6-ring def.1

[a] Relative band intensities are normalized to a value of 100 for the 568 cm^{-1} band in each spectrum.

In the case of [Ni^{II}TMTAA] the solid-state RR spectra exhibit rather different behavior, which is to be understood in terms of the lower symmetry (C_{2v}) and the shift of absorption band I to lower energy, relative to [Ni^{II}TAA], and band II to higher wavenumber. Excitation at 514.5 nm is midway between bands I and II and leads to a RR spectrum in which the lower wavenumber bands are more intense than those above 1000 cm^{-1}. The strong bands below 900 cm^{-1} are mostly attributable to the in-plane deformations of the benzene and imine rings, reflecting the distortions that must occur in the lowest energy $^1B_{2u}$ state. The high-wavenumber bands increase in intensity with shorter wavelength excitation; 457.9 nm is close to the maximum of band II, which appears as a shoulder in the poorly resolved solid-state absorption spectrum. In all RR spectra there are some bands which can only be assigned to vibrations of *u*-type, which become allowed as a consequence of the lower molecular symmetry.

SERRS Spectra. The SERRS spectra of [Ni^{II}TAA] and [Ni^{II}TMTAA], measured with various Ag electrode poten-

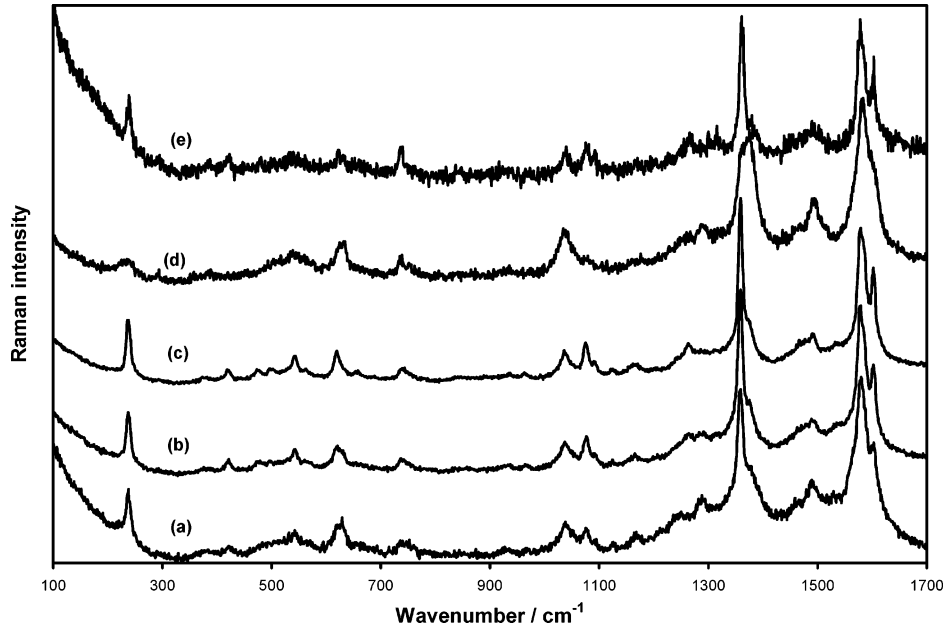

Figure 6. SERRS spectra of [Ni^{II}TAA] recorded with 514.5 nm excitation at (a) −0.1, (b) −0.3, (c) −0.6, (d) −0.9, and (e) −1.1 V vs Ag/AgCl.

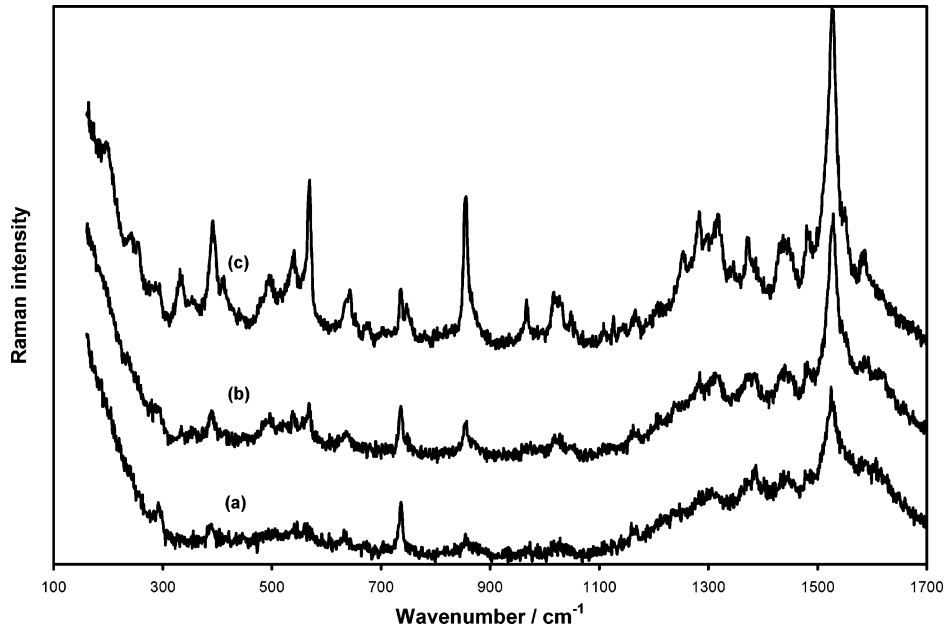

Figure 7. SERRS spectra of [Ni^{II}TMTAA] recorded with 514.5 nm excitation at (a) −0.1, (b) −0.3, and (c) −0.6 V vs Ag/AgCl.

tials, using 514.5 nm excitation, are shown in Figures 6 and 7; and band wavenumber measurements are listed together with the RR data and assignments in Tables 6 and 7. The [Ni^{II}TAA] SERRS band positions are mostly within 5 cm^{-1} of those in the RR spectra, and relative band intensities in the spectrum obtained at a potential of −0.6 V are mostly similar to those in the RR spectrum. There are decreases in the relative intensities of the 238, 421, 542, and 1075 cm^{-1} bands, which become more pronounced at increasingly positive potential. At −0.3 V there is a slight increase in the relative intensity of the 1579 cm^{-1} band, and at −0.1 V the lower wavenumber bands are much less intense, except the 239 cm^{-1} band which is still quite strong. The most striking changes are the increased intensities of the 620, 1040, and 1580 cm^{-1} bands. The Raman signal decreases with increasingly positive potential. Plots of absolute band intensities vs potential and also band intensities relative to the band at 1040 cm^{-1} (Figure 8) pass through a maximum near −0.6 V (fwhm 0.6 V).

In the case of [Ni^{II}TMTAA] the SERRS spectra also resemble the RR spectrum excited at 514.5 nm, although several bands are shifted, in this instance by up to 15 cm^{-1} compared with the RR spectra. Variation of the electrode potential also causes major changes in the relative band intensities. At −0.3 V, the signal-to-noise ratio is poorer and there are a few relative intensity changes; in particular, the 290 cm^{-1} band increases in intensity, the 567 cm^{-1} band loses intensity, and the 733 cm^{-1} band increases in relative intensity. As the potential is switched to −0.1 V, the 329 cm^{-1} band disappears and there are decreases in the relative

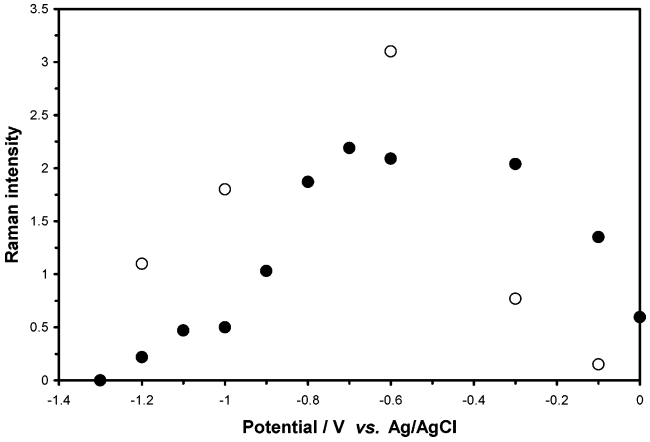

Figure 8. Plots of Raman intensity vs potential for the 1361 cm^{-1} band of [Ni^{II}TAA] (●) and the 850 cm^{-1} band of [Ni^{II}TMTAA] (○).

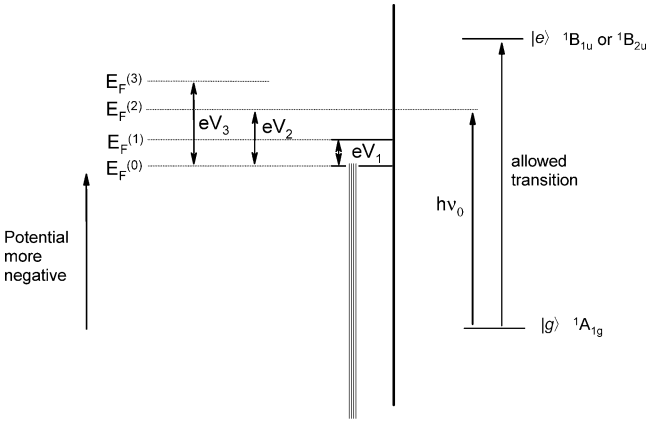

Figure 9. Energy level diagrams for TAA complexes interacting with a silver surface, at successively more negative applied potentials $V_1 > V_2 > V_3$, which shifts the Fermi level to higher energy. At V_2 the Raman intensity contribution from the CT mechanism with 514.5 nm excitation reaches a maximum at V_{max}. The intensity is borrowed from the intense $^1B_{1u} \leftarrow {}^1A_{1g}$ transition by vibronic coupling between the Fermi level and a higher energy excited state.

intensities of the 390, 567, and 853 cm^{-1} bands. The band at 733 cm^{-1}, which appears to become more intense, is attributed to Raman scattering from the Teflon insulating sheath. Plots of absolute band intensities vs potential (and also band intensities relative to the 733 cm^{-1} band) pass through a maximum near −0.7 V (fwhm 0.8 V) for the [Ni^{II}TMTAA] complex. The close correspondence of V_{max} with the [Ni^{II}TAA] complex value is perhaps not surprising given its very similar absorption spectrum.

The spectra indicate that the molecules are weakly chemisorbed on the Ag surface and that they retain their geometry, although [Ni^{II}TMTAA] is perturbed to a greater degree on adsorption. Similar behavior was observed for the free ligands[8] and has also been witnessed in SERRS studies of metal bipyridine complexes adsorbed on Ag electrodes[32,33] and colloids,[34] but contrasts with the observations reported for SERRS studies of porphyrins which show evidence for chemisorption with coordinated surface Ag atoms.[35−37] Dramatic potential-dependent intensity changes were observed in the SERRS spectra of both complexes, and the maxima in the plots of absolute band intensities vs potential intensities are close to the potential of zero charge for the silver electrode in water.[38] We do not expect the TAA complexes to be reversibly adsorbed under these conditions, and we can rule out the possibility that the complexes are being reduced, since the redox potential is expected at −1.8 V. Chronocoulometric data for [Ni^{II}TMTAA] show a small capacitance spike at −1.0 V which is probably caused by a rearrangement of the adsorbed layer,[39] which would lead to changes in the relative intensities of the bands, dependent on their symmetry. According to surface selection rules proposed by Creighton,[2,40] a flat orientation of the adsorbed molecule, with the molecular plane parallel to the surface, would lead to preferential enhancement of out-of-plane vibrations. Conversely, a perpendicular edge-on orientation would favor in-plane modes. If the adsorbate were to adopt a tilted orientation, then both in-plane and out-of-plane vibrations would have components in the direction perpendicular to the surface, and this would result in equal surface enhancement. Such behavior has, however, been found for free-base porphyrins.[41] However, in the present case the flat orientation can be ruled out on the grounds that no out-of-plane modes are expected (from the ab initio calculations) above 1200 cm^{-1}, where the major spectral changes occur. Therefore, it seems unlikely that changes in molecular orientation, within the framework of the electromagnetic (EM) SERS mechanism, are responsible for the potential-dependent intensity changes.

The potential dependence can alternatively be explained in terms of the chemical or charge transfer (CT) contribution to surface enhancement, several examples of which have recently been discussed in the literature.[42−47] According to the CT mechanism[3,48,49] the interaction of adsorbate energy levels with those of the silver surface is represented by a charge transfer either in the direction adsorbate-to-metal or vice versa. For simplicity we consider the former case only, as shown in Figure 9. Laser excitation is either off-resonance

(32) Stacy, A. M.; van Duyne, R. P. *Chem. Phys. Lett.* **1983**, *102*, 365.
(33) Virdee, H. R.; Hester, R. E. *J. Phys. Chem.* **1984**, *88*, 451.
(34) Dines, T. J.; Peacock, R. D. *J. Chem. Soc., Faraday Trans. 1* **1988**, *84*, 3445.
(35) Itoh, K.; Sugii, T.; Kim, M. *J. Phys. Chem.* **1988**, *92*, 1568.
(36) Chen, J.; Hu, J. M.; Xu, Z. S.; Sheng, R. S. *Appl. Spectrosc.* **1993**, *47*, 292.
(37) Tai, Z. H.; Zhang, J. F.; Gao, J. S.; Xue, G. *J. Mater. Chem.* **1993**, *3*, 417.
(38) Trasatti, S. *Electrochim. Acta* **1992**, *37*, 2137.
(39) Muszalska, E.; Bilewicz, R. *Electroanalysis* **1996**, *8*, 173.
(40) Creighton, J. A. *Surf. Sci.* **1983**, *124*, 209.
(41) Vlčková, B.; Matějka, P.; Pančoška, P.; Baumruk, V.; Král, V. *Inorg. Chem.* **1991**, *30*, 4103.
(42) Brolo, A. G.; Irish, D. E. *J. Electroanal. Chem.* **1996**, *414*, 183.
(43) Lombardi, R.; Birke, R. L.; Sanchez, L. A.; Bernard, I.; Sun, S. C. *Chem. Phys. Lett.* **1984**, *104*, 240.
(44) Rubim, J. C.; Corio, P.; Ribeiro, M. C. C.; Matz, M. *J. Phys. Chem.* **1995**, *99*, 15765.
(45) Rubim, J. C.; Temperini, M. L. A.; Corio, P.; Sala, O.; Jubert, A. H.; Chacon-Villalba, M. E.; Aymonino, P. Y. *J. Phys. Chem.* **1995**, *99*, 345.
(46) Corio, P.; Rubim, J. C. *J. Phys. Chem.* **1995**, *99*, 13217.
(47) Corio, P.; Rubim, J. C. *J. Raman Spectrosc.* **1997**, *28*, 235.
(48) Lombardi, J. R.; Birke, R. L.; Lu, T.; Xu, J. *J. Chem. Phys.* **1986**, *84*, 4174.
(49) Birke, R. L.; Lombardi, J. R. In *Spectroelectrochemistry: Theory and Practice*; Gale, R. J., Ed.; Plenum: New York, 1988; Chapter 6, p 263.

or close to resonance with the lowest energy electric-dipole-allowed electronic transition in the complex. The radiation excites electrons largely confined to the adsorbate energy levels, in the ground state $|g\rangle$, into vacant metal energy levels near the Fermi level, with high cross section, by a CT process. When the applied voltage becomes more negative ($V_1 \leq V_2 \leq V_3$), the Fermi level is shifted to higher energy and the CT transition moves in (V_2) and then out of resonance (V_3). This gives the characteristic peaked intensity vs potential plot (in this case $V_2 = V_{max}$). Conversely, for a given excitation energy $h\nu_i$ the intensity will maximize at a particular potential $V_{max}{}^i$. The intensity of the spectrum derives from vibronic coupling with the allowed $|e\rangle \leftarrow |g\rangle$ transition, which is more significant than in the RR case as the Fermi level is much closer in energy to the excited state $|e\rangle$. Assuming adsorbate-to-metal CT, the Herzberg−Teller term only permits B-term vibronic coupling which would be expected to enhance symmetric and nonsymmetric modes, analogous to the RR spectrum, as observed.

We propose that the intensity/potential variation observed for both complexes is consistent with this CT picture. Furthermore, the changes at more positive potentials are evidence for the emergence of the underlying broad and fairly weak EM-SERS spectrum (largely a_g bands) as the CT-SERS contribution decays (consisting of both a_g and b_{3g} bands). The spectra observed for the complexes close to V_{max} are very similar to what would be expected from the type of B-term enhancement (from the Herzberg−Teller term) found for adsorbate-to-metal direction of charge transfer, and also found in the RR spectra. A wavelength-dependence study was carried out at a fixed potential (−0.6 V vs Ag/AgCl) with 514.5, 528.7, and 613.6 nm excitation. Using 514.5 nm excitation the SERRS spectrum is similar to the RR spectrum, although at 528.7 nm the low-wavenumber bands appear to lose intensity relative to those in the high-wavenumber region; for example, the 566 cm^{-1} band clearly loses appreciable intensity. With 613.6 nm excitation the high-wavenumber bands disappear, leaving mainly bands below 900 cm^{-1} of which the most intense are those at 196 and 636 cm^{-1}, attributed to ring deformations of a_g and b_{3g} symmetry. The intense 636 cm^{-1} band indicates the importance of vibronic coupling through the B term.

In summary, we believe our potential-dependent data is best explained by the CT contribution rather than a change in adsorbate orientation, which would alter the contribution from the EM mechanism, or an alteration in surface coverage. The fact that the Ni(II) complexes show much less intensity variation with potential than the free ligands reported in our previous paper may be explained by either (i) a greater degree of interaction between the surface and the metal complexes, as observed in isotherm studies,[50,51] or (ii) the more accessible adsorbate excited-state energy levels in the complexes. The dominance of CT-SERS rather than SERRS is a little surprising given that the exciting wavelengths are close to preresonance, although the distinct potential dependence observed is not consistent with SERRS.[52] We are aware of a complication due to the possibility of potential-dependent formation of aggregates on the metal surface, as reported in the elegant work of Akins et al.[53] Nevertheless, we did not observe any unusual new bands and it is significant that electrode roughening was needed in the present study, whereas aggregate RR spectra are usually observed on a smooth electrode.

Conclusion

In this study we have reported the first vibrational band assignments of these complexes based on ab initio calculations at the hybrid SCF-DFT level. The particular significance of this approach is that normal coordinate analysis of large molecules is not always straightforward and, given the selective nature of the RR effect, not all Raman-active vibrations are actually observed. Ab initio calculations therefore provide a valuable aid to the interpretation of vibrational spectra. SERS spectra of [Ni^{II}TAA] showed very few differences from the RR spectra in terms of band wavenumber positions, although potential-dependent variations of relative band intensities were observed. The results can understood in terms of (a) weak chemisorption of these molecules, with no apparent lowering of symmetry upon adsorption, and (b) surface enhancement which is due largely to the CT contribution. Variation of SERS band intensities as a function of electrode potential can be understood in terms of current ideas of the charge-transfer contribution to SERS. The results of this study are a promising indication that the combination of SERS data with IR, RR, and ab initio calculations will be fruitful in providing new insights into the behavior of transition metal TAA complexes adsorbed at electrode surfaces.

Acknowledgment. The authors thank the EPSRC for a research grant for the support of S.B.E. and C.I.S. (Grant GR/J/79775). We thank also Drs. Bruce Alexander and Andrew P. Taylor for helpful discussions.

Supporting Information Available: Listings of further details related to the ab initio calculations. This material is available free of charge via the Internet at http://pubs.acs.org.

IC026216E

(50) Drew, M. G. B.; Jutson, N. J.; Mitchell, P. C. H. *J. Mater. Chem.* **1992**, *2*, 817.
(51) Drew, M. G. B.; Jutson, N. J.; Mitchell, P. C. H.; Potter, R. J.; Thompsett, D. *J. Chem. Soc., Faraday Trans.* **1993**, *89*, 3963.
(52) Kudelski, A.; Bukowska, J. *Chem. Phys. Lett.* **1996**, *253*, 246.
(53) Akins, D. L.; Macklin, J. W. *J. Phys. Chem.* **1989**, *93*, 5999.